Scientific Research Publishing

Engineering, 2026, 18(1), 1-15
https://www.scirp.org/journal/eng
ISSN Online: 1947-394X
ISSN Print: 1947-3931

Research on the Independence of the Cylinder Shaft with a Linter Machine

Avazbek Obidov*, Akhrorbek Abdurasulov

Faculty of Mechanics, Namangan State Technical University, Namangan, Uzbekistan
Email: *obidovavazbek66@gmail.com

How to cite this paper: Obidov, A. and Abdurasulov, A. (2026) Research on the Independence of the Cylinder Shaft with a Linter Machine. *Engineering*, **18**, 1-15.
https://doi.org/10.4236/eng.2026.181001

Received: December 18, 2025
Accepted: January 17, 2026
Published: January 20, 2026

Abstract

In this article, theoretical studies were conducted to determine the bending strength of a saw-toothed drum shaft under load based on bending moments and displacement diagrams. The diagrams constructed as a result of theoretical work show that in rigidly supported shafts, the maximum bending moments are concentrated mainly in the support areas, while in freely supported shafts, the largest moment values are formed in the central part. This fact confirms that the type of support directly affects the location of stresses. According to the displacement diagrams, the greatest deflection of the shaft was observed in zones with intensive load effects. The diagrams of normal and equivalent stresses made it possible to identify the most dangerous sections of the shaft. This fact is of great importance in material selection and determining the safety margin. The diagrams constructed in the MathCad environment confirmed the consistency and stability of the results obtained on the basis of theoretical calculations and demonstrated the suitability of the developed mathematical model for practical application.

Keywords

Linter Machine, Grain, Vibration, Strength, Resource-Saving Shaft, Saw Cylinder, Loading, Saw Drum, Displacement, Bending, Moments

1. Introduction

In this study, it was planned to carry out strength testing of the linter machine saw drum shaft based on a modern program. In this case, by preparing the existing working linter shaft with grooves and a central groove on the surface, the turning moment, vibration, and vertical longitudinal deflection of the saw cylinder shaft change as a result of mass lightening [1]-[3].

The objectives of the conducted research are as follows:

- measurement of the turning moment of the saw cylinder shaft;
- determination of the deflection of the saw cylinder shaft;
- reduction of vibration of the saw cylinder shaft;
- analysis of the power consumption of the linter machine shaft.

The purpose of the research is to determine the kinematic and dynamic capabilities of the proposed resource-saving saw cylinder shaft using experimental studies and its compliance with the laws obtained on the basis of theoretical research.

Analysis of the bending strength of a saw drum shaft under load (**Figure 1**). When determining the bending strength of a saw drum shaft under the influence of loads (vibration, saw drum, and grain mass) that occur together with the grain flow during operation, we consider the process of applying various loads [4].

The evenly distributed force acting on the shaft:

$$q = -\gamma \cdot by \tag{1}$$

$$k = \sqrt[4]{\frac{\gamma b}{4EJ}} \tag{2}$$

Wall stiffness coefficient (1/m); γ: specific gravity of steel; b: the radius of the shaft; E: modulus of elasticity; J: moment of inertia.

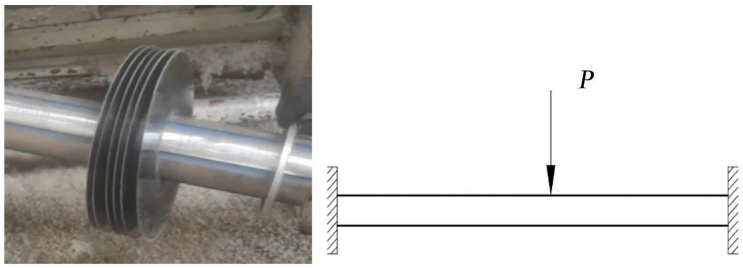

Figure 1. Diagram of a sawmill drum shaft and the effect of loading on it.

Expression (2) is the ratio of the stiffness of the shaft to the resistance of the cotton flow to the base. We assume that the weight of the shaft is balanced by the force exerted by the cotton flow [5], therefore,

$$Y^{(\mathrm{IV})} + 4k^4 y = \frac{q}{EJ} \tag{3}$$

From the expression $q = 0$, we can infer.

We calculate the equilibrium state with $p = 0$ along the displacement y-direction, and the general solution of expression (3) for the additional displacement is determined as follows:

$$\begin{aligned} y = {} & C_1 \sin(kz)\,\mathrm{sh}(kz) + C_2 \sin(kz)\,\mathrm{ch}(kz) \\ & + C_3 \cos(kz)\,\mathrm{sh}(kz) + C_4 \cos(kz)\,\mathrm{ch}(kz) \end{aligned} \tag{4}$$

where, $\mathrm{sh}(kz)$ and $\mathrm{ch}(kz)$ are the hyperbolic sine and hyperbolic cosine functions, respectively.

$$\begin{cases} y' = (C_2 - C_3)k\sin(kz)\mathrm{sh}(kz) + (C_1 - C_4)k\sin(kz)\mathrm{sh}(kz) \\ \quad + (C_1 - C_4)k\sin(kz)\mathrm{sh}(kz) + (C_2 - C_3)k\sin(kz)\mathrm{sh}(kz) \\ y'' = 2C_1k^2\cos(kz)\mathrm{ch}(kz) + 2C_2k^2\cos(kz)\mathrm{sh}(kz) - 2C_3k^2\sin(kz)\mathrm{ch}(kz) \\ \quad - 2C_3k^2\sin(kz)\mathrm{ch}(kz) - 2C_4k^2\sin(kz)\mathrm{sh}(kz) \\ y''' = 2(C_2 - C_3)k^3\cos(kz)\mathrm{ch}(kz) + 2(C_1 - C_4)k^3\cos(kz)\mathrm{sh}(kz) \\ \quad - 2(C_1 - C_4)k^3\sin(kz)\mathrm{ch}(kz) - 2(C_2 + C_3)k^3\sin(kz)\mathrm{sh}(kz) \end{cases} \quad (5)$$

The origin of the coordinate system is found at the point $z = 0$, that is, the point where the force P is applied. Since the case is symmetrical, the transverse force Q for the right-hand section is:

$$Q = \frac{P}{2} \quad (6)$$

Also,

$$EJy''' = \frac{P}{2};\quad y' = 0;\quad y''' = \frac{P}{2EJ}$$

So, using the four boundary conditions C_1, C_2, C_3, and C_4, we define the invariants if $z = l$, $M = EJy'' = 0$ and $Q = EJy'' = 0$.

$$C_2 + C_3 = 0$$

$$C_2 + C_3 = \frac{P}{4EJk^3}$$

$$C_1\cos(kl)\mathrm{ch}(kl) + C_2\cos(kl)\mathrm{ch}(kl) - C_3\sin(kl)\mathrm{ch}(kl) - C_4\sin(kl)\mathrm{ch}(kl) = 0$$

$$C_1\left(\cos(kl)\mathrm{sh}(kl) - \sin(kl)\mathrm{ch}(kl)\right) + C_2\left(\cos(kl)\mathrm{ch}(kl) - \sin(kl)\mathrm{sh}(kl)\right)$$
$$+ C_3\left(-\cos(kl)\mathrm{ch}(kl) - \sin(kl)\mathrm{sh}(kl)\right) + C_4\left(-\cos(kl)\mathrm{sh}(kl) - \sin(kl)\mathrm{ch}(kl)\right) = 0$$

From these expressions,

$$C_2 = \frac{P}{8EJk^3}\cdot\frac{\mathrm{sh}^2(kl) + \sin^2(kl)}{\mathrm{sh}(kl)\mathrm{ch}(kl) + \sin(kl)\cos(kl)}$$

$$C_2 = \frac{P}{8EJk^3};\quad C_3 = \frac{P}{8EJk^3}$$

$$C_4 = \frac{P}{8EJk^3}\cdot\frac{\mathrm{ch}^2(kl) + \cos^2(kl)}{\mathrm{sh}(kl)\mathrm{ch}(kl) + \sin(kl)\cos(kl)}$$

To determine the bending moment y'', we calculate it by substituting the regular product:

$$M = EJy'' \quad (7)$$

We determine the bending moment by putting it into the expression:

$$M = \frac{P}{4k}\left[\frac{\mathrm{sh}^2(kl) + \sin^2(kl)}{\mathrm{sh}(kl)\mathrm{ch}(kl) + \sin(kl)\cos(kl)}\cos(kz)\mathrm{ch}(kz)\right.$$
$$\left. - \cos(kz)\mathrm{sh}(kz) - \cos(kz)ch(kz) + \frac{\mathrm{ch}^2(kl) + \cos^2(kl)}{\mathrm{sh}(kl)\mathrm{ch}(kl) + \sin(kl)\cos(kl)}\right] \quad (8)$$

When a saw drum shaft, the contour of which is reinforced in two ways, is subjected to a uniformly distributed pressure P, we determine its deflection and stresses in a freely supported state (**Figure 1**) [6]. The radius of the saw disk is R, and the thickness is h. We determine the force Q that arises in the supports under the influence of the load due to the flow of grain. For a shaft with a radius of r in the central part (**Figure 2**) [7], since the outer shaft is fixed, the equilibrium equation is as follows:

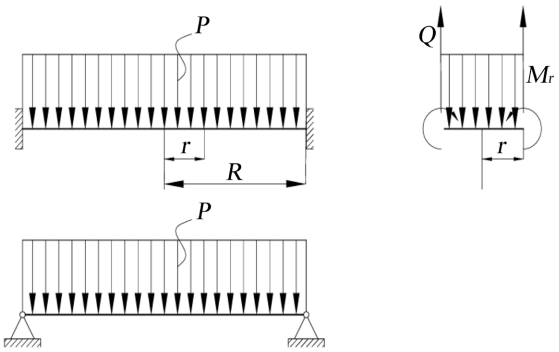

Figure 2. Diagram of the force acting on the shaft.

We determine the forces at the support points of the saw blade shaft as follows:

$$Q \cdot 2 \cdot \pi \cdot r = P \cdot \pi \cdot r^2 \quad \text{or} \quad Q = \frac{P \cdot r}{2}$$

Let's consider the fastening cases separately.

1) The shaft is fully tightened:

$$\left.\begin{aligned} M_r &= D \cdot \left(\frac{d\vartheta}{dt} + \mu \cdot \frac{\vartheta}{r} \right) \\ M_t &= D \cdot \left(\mu \cdot \frac{d\vartheta}{dt} + \frac{\vartheta}{r} \right) \end{aligned}\right\} \tag{9}$$

According to formula (9), the bending moments are:

$$\left.\begin{aligned} M_r &= \frac{\rho}{16}\left[R^2 (1+\mu) - r^2 (3+\mu) \right] \\ M_t &= \frac{\rho}{16}\left[R^2 (1+\mu) - r^2 (1+3\mu) \right] \end{aligned}\right\} \tag{10}$$

$\vartheta = \frac{\mathrm{d}\delta}{\mathrm{d}t}$, we determine from the expression:

$$\delta = \frac{\rho}{16D}\left[C_3 - \frac{1}{2} R^2 r^2 \frac{r^4}{4} \right]$$

where the constant C_3 is determined from the condition that the displacement δ in the contour is equal to zero.

$$\left.\begin{aligned} C_3 &= \frac{1}{4} R^4 \\ \delta &= \frac{\rho}{64D}\left(R^2 - r^2 \right)^2 \end{aligned}\right\} \tag{11}$$

2) The case of a freely supported shaft with a saw blade:

In this case, the radial stress σ_r (or moment M_r) on the shaft is zero. Therefore, according to (9) at r = R:

$$\frac{d\vartheta}{dr}+\frac{\mu\vartheta}{r}=0$$

This is found in the C_1.

$$C_1-\frac{3pR^2}{16D}+\mu\left(C_1-\frac{pR^2}{16D}\right)=0$$

From this:

$$C_1=\frac{pR^2}{16D}\cdot\frac{3+\mu}{1+\mu}$$

Angle:

$$\vartheta=\frac{p}{16D}\left[\frac{3+\mu}{1+\mu}R^2r^2-r^2\right]$$

According to expressions (9), we determine the bending moments: These moments are given for the shaft and the saw blade.

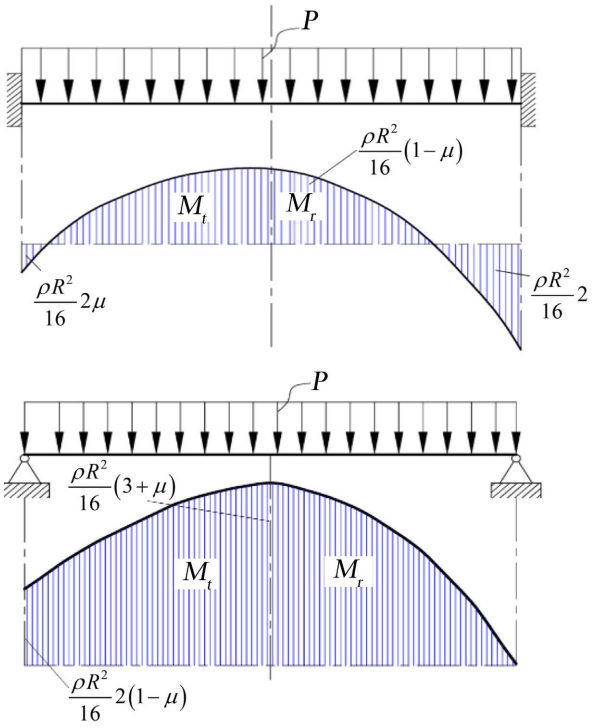

Figure 3. Bending moment diagram under the influence of a grain flow falling on a shaft.

$$\left.\begin{aligned}M_r&=\frac{\rho}{16}(3+\mu)R^2-r^2\\M_t&=\frac{\rho}{16}(3+\mu)R^2-\frac{3+\mu}{1+\mu}r^2\end{aligned}\right\}\qquad(12)$$

The shift expression has the following form:

$$\delta = \frac{\rho}{16D}\left[C_2 - \frac{3+\mu}{1+\mu}\frac{R^2 r^2}{2} + \frac{r^4}{4}\right]$$

The constant C_2 is chosen from the condition that the displacement on the contour is zero,

$$C_2 = \frac{R^4}{4}\frac{5+\mu}{1+\mu}$$

From this:

$$\delta = \frac{P}{16D}\left[\frac{1}{4}\frac{5+\mu}{1+\mu}R^4 - \frac{1}{2}\frac{3+\mu}{1+\mu}R^2 r^2 + \frac{1}{4}r^4\right] \tag{13}$$

According to expressions (11) and (13), the bending moment diagrams shown in **Figure 3** are constructed.

In the case of a compressed shaft [8], the greatest tensile stresses occur on the upper surface near the end.

$$\sigma_1 = \sigma_r = \frac{2\rho R^2}{16}\frac{6}{h^2}, \quad \sigma_2 = \sigma_t = \frac{2\mu\rho R^2}{16}\frac{6}{h^2}, \quad \sigma_3 = 0$$

Equivalent voltage:

$$\sigma_{ekv} = \sigma_1 - k\sigma_3 = \frac{3}{4}\frac{\rho R^2}{h^2}$$

The greatest tensile stresses of a freely supported shaft are generated at the bottom surface in the center:

Here,

$$\sigma_1 = \sigma_r = \frac{3+\mu}{16}\frac{\rho R^2 6}{h^2}, \quad \sigma_3 = 0$$

Equivalent voltage:

$$\sigma_{ekv} = \sigma_1 - k\sigma_3 = \frac{3}{8}(3+\mu)\frac{\rho R^2}{h^2}$$

In the first and second cases, the largest deviations according to expressions (2.17) and (2.19) will be as follows:

$$\text{a)} \quad \delta = \frac{P}{64D}; \text{ b)} \quad \delta = \left[\frac{5+\mu}{1+\mu}\frac{PR^4}{64D}\right]$$

Above, we considered the cases of non-bending extension of the shell (the theory without moments) and bending of the saw blade without stretching. Now we turn to a more general case in which both bending moments and normal forces arise in the shell sections.

We consider the problem of determining the stresses in a symmetrically loaded saw blade shaft. This problem is solved on the basis of the same assumptions as in the problem of shaft bending, namely, the hypothesis of the invariance of the normal and the assumption that the layers of the saw blade drum do not press on each other.

2. Determination of Stresses and Displacements due to the Movement of a Grain Stream in a Circular Saw Blade Shaft

A circular saw blade cylinder with radius R and thickness h of constant radius is subjected to a load symmetrically along a certain axis (Figure 4). The deformations and stresses generated in the shaft also naturally have symmetry along the axis and form a deformed cylindrical body of revolution [9]. The shape of this body is completely determined by the shape of the bent cylinder body.

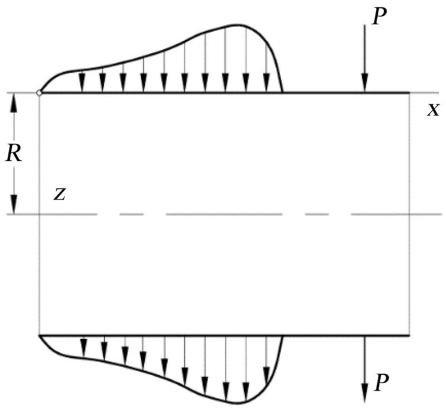

Figure 4. Diagram of the saw drum shaft under an axially symmetrical load.

We define the radial displacement by ϖ [10] as the angle of deviation of the tangent drawn to the center of the shaft (Figure 5).

$$\frac{\mathrm{d}\varpi}{\mathrm{d}x} = \vartheta \tag{14}$$

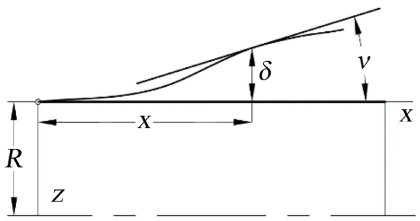

Figure 5. Scheme of displacement of the shaft under load relative to the supports.

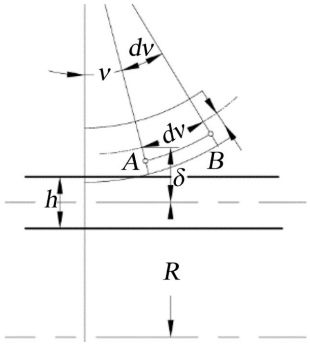

Figure 6. Elongation diagram resulting from the influence of the AB layer on cotton flow.

We calculate the displacement ϖ outward from the shaft axis, *i.e.*, outward. The relative elongation ε_x of the section AB (Figure 6) at a distance z from the midsurface consists of two components: the elongation of the midsurface of the shaft ε_0; and the additional elongation resulting from the bending of the frame.

The last addition looks like this: $z = \frac{\mathrm{d}\vartheta}{\mathrm{d}x}$. Thus, the full extension of layer AB will have the following appearance:

$$\varepsilon_x = \varepsilon_0 z + \frac{\mathrm{d}\vartheta}{\mathrm{d}x} \tag{15}$$

Stretching along a circular path

$$\varepsilon_y = \frac{\varpi}{R} \tag{16}$$

These strains produce stresses σ_x and σ_y, which are related to each other according to Hooke's law.

$$\sigma_x = \frac{E}{1-\mu^2}\left(\varepsilon_x + \mu\varepsilon_y\right), \quad \sigma_y = \frac{E}{1-\mu^2}\left(\varepsilon_y + \mu\varepsilon_x\right)$$

Or according to expressions (15) and (16),

$$\left.\begin{aligned} \sigma_x &= \frac{E}{1-\mu^2}\left[\varepsilon_0 + \mu\frac{\varpi}{R} + z = \frac{\mathrm{d}\vartheta}{\mathrm{d}x}\right] \\ \sigma_y &= \frac{E}{1-\mu^2}\left[\mu\varepsilon_0 + \frac{\varpi}{R} + \mu z = \frac{\mathrm{d}\vartheta}{\mathrm{d}x}\right] \end{aligned}\right\} \tag{17}$$

Bending moments and normal forces are generated in the shaft sections. They are determined by the stresses σ_x and σ_y, just as we did for a circular shaft.

Bending moments and normal forces are generated in the shaft sections. They are determined by the stresses σ_x and σ_y, just as we did for a circular shaft.

Let's consider a cylindrical sawtooth drum element of dimensions d_x d_y (Figure 7).

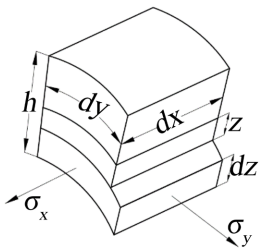

Figure 7. Diagram of determining stresses in the sawn drum layer.

The forces on the surfaces hdy and hdx, the cross-sectional arcs assigned to the unit, will be:

$$T_x = \int_{-h/2}^{+h/2} \sigma_x \cdot \mathrm{d}z$$

$$T_y = \int_{-h/2}^{+h/2} \sigma_y \cdot \mathrm{d}z$$

We determine the bending moments in these sections:

$$M_x = \int_{-h/2}^{+h/2} \sigma_x \cdot z \cdot dz$$

$$M_y = \int_{-h/2}^{+h/2} \sigma_y \cdot z \cdot dz$$

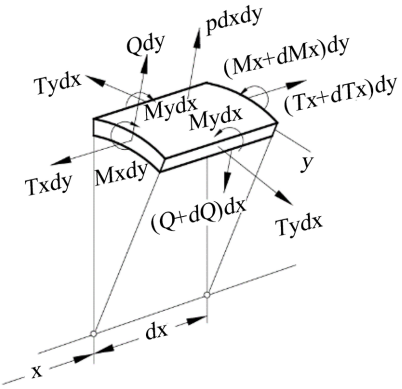

Figure 8. Diagram of forces acting on a shaft for shear.

Taking into account expressions (15) and (17), we determine the forces T_x and T_y and the moments M_x and M_y depending on the displacement ϖ :

$$T_x = \frac{Eh}{1-\mu^2}\left(\varepsilon_0 + \mu\frac{\varpi}{R}\right), \quad T_y = \frac{Eh}{1-\mu^2}\left(\frac{\varpi}{R} + \mu\varepsilon_0\right) \tag{18}$$

$$M_x = D\frac{d^2\varpi}{dx^2}, \quad M_x = \mu D\frac{d^2\varpi}{dx^2} \tag{19}$$

Here, as before

$$D = \frac{Eh^2}{12\left(1-\mu^2\right)}$$

Now, we turn to the equilibrium equations. We again consider a shaft element with dimensions h, dx, dy, and apply to its edges the resultant forces and moments equal to the values T_x, T_y, M_x, and M_y multiplied by dy and dx, respectively (**Figure 8**). In addition to the four force factors listed, we also apply the transverse force Q dy. The external forces are characterized by the pressure $P = P(x)$.

When moving from the edge with coordinate x to the edge with coordinate $x + dx$, the forces increase accordingly. In sections with axis Y, the force factors remain the same due to the symmetry properties.

Projecting the forces along the shaft axis, we obtain:

$$dT_x = 0, \quad T_x = \text{const}$$

This means that the shear force is determined by the loading conditions at the three ends of the shaft. In what follows, these conditions are assumed to be given, and the force T_x is assumed to be known.

Projecting the forces in the radial direction, we obtain the second equation of equilibrium.

$$-T_y dx\frac{dy}{R} - dQdy + Pdxdy = 0,$$

Or,

$$\frac{dQ}{dx} = P - \frac{T_y}{R} \tag{20}$$

The third equation of equilibrium was obtained by setting the sum of all moments of forces about the axis (relative to the normal to the arc of the section) to zero:

$$Qdydx = dM_x dy$$

Here,

$$Q = \frac{dM_x}{dx} \tag{21}$$

The remaining equilibrium equations are automatically satisfied for any values of the acting forces due to symmetry.

Now, we rewrite the obtained equations. We subtract ε_0 from Equation (18), and subtract the shear force Q from Equations (20) and (21). Then we get:

$$\left.\begin{aligned} T_y &= \frac{Eh}{R}\varpi + \mu T_x \\ \frac{\mathrm{d}^2 M_x}{\mathrm{d}x^2} &= p - \frac{T_y}{R} \end{aligned}\right\} \tag{22}$$

We can extract T_y from these equations:

$$\frac{d^2 M_x}{dx^2} = p - \frac{Eh}{R^2}\varpi + \frac{\mu}{R}T_x$$

If we use the first expression of Equation (19) and eliminate the bending moment M_x, we obtain an equation for one unknown—the displacement ϖ:

$$\frac{d^4 M_x}{dx^4} + 4k^4\varpi = \frac{P}{D} + \frac{\mu T_x}{RD} \tag{23}$$

Here,

$$4k^4 = \frac{Eh}{R^2 D} = \frac{12\left(1-\mu^2\right)}{R^2 h^2} \tag{24}$$

$Y^{(\mathrm{IV})} + 4k^4 y = \frac{q}{EJ}$. The differential equation is the same as the equation for the bending of a shaft on an elastic base.

The shaft shell can be viewed as a set of mutually bending lines connected by elastic forces. Under symmetrical loading, all lines bend equally, and the radial component of the force T_y at each section is proportional to the deflection ϖ, as in a beam on an elastic foundation.

Valga tushgan yuklanishdagi kuchni aniqlash mumkin.

$$Q = D\frac{d^3\varpi}{dx^3} \tag{25}$$

The largest stresses are determined by the following expressions, where $z = +h/2$ or $z = +h/2$.

$$\sigma_x = \frac{E}{1-\mu^2}\left[\left(\varepsilon_0 + \mu\frac{\varpi}{R}\right) \pm \frac{h}{2}\frac{\mathrm{d}^2\varpi}{\mathrm{d}x^2}\right], \quad \sigma_y = \frac{E}{1-\mu^2}\left[\left(\mu\varepsilon_0 + \frac{\varpi}{R}\right) \pm \mu\frac{h}{2}\frac{\mathrm{d}^2\varpi}{\mathrm{d}x^2}\right]$$

If we subtract the values here using expressions (18) and (19):

$$\sigma_x = \frac{T_x}{h} \pm \frac{6M_x}{h^2}, \quad \sigma_y = \frac{T_y}{h} \pm \frac{6M_x}{h^2} \tag{26}$$

Thus, the internal forces are expressed in terms of the displacement *w*, from which the stresses are then determined.

$$\varpi = \mathrm{e}^{-kx}\left(C_1 \sin kx + C_2 \cos kx\right) + \mathrm{e}^{+kx}\left(C_3 \sin kx + C_4 \cos kx\right) + \varpi^* \tag{27}$$

where ϖ^* is a special solution, which is found depending on the law of variation of P along the derivative.

To determine the four constant parameters, it is necessary to specify four boundary conditions and then solve the system of four equations. In most cases, this system is said to be weakly coupled and decomposes into two systems of two equations. With sufficient accuracy, the constants C_1 and C_2 are determined independently of the constants C_3 and C_4.

This is explained as follows: the adders entering the function ϖ (27) have different properties. The first adder

$$\mathrm{e}^{-kx}\left(C_1 \sin kx + C_2 \cos kx\right)$$

Expressed as a rapidly decaying function. The second additive

$$\mathrm{e}^{+kx}\left(C_3 \sin kx + C_4 \cos kx\right)$$

Expressed as a rapidly increasing function.

If the cylinder length *l* is large enough and the function

$$\mathrm{e}^{-kx}\left(C_1 \sin kx + C_2 \cos kx\right)$$

For values of *x* close to *l*, the function is almost zero, so the deformation at the second end of the cylinder can be considered independent of the conditions around the first end. Thus, for a sufficiently long cylinder, the stress state in the region of small *x* is $\mathrm{e}^{+kx}\left(C_3 \sin kx + C_4 \cos kx\right)$, can be analyzed by ignoring the increasing function, that is, $C_1 = C_2 = 0$ is accepted as. In this way, assuming $C_3 = C_4 = 0$ and retaining only the increasing integral, it is possible to analyze the stress state of the cylinder at values of x close to *l*.

In the calculations, the graphs are constructed under the influence of the following parameters.

1) Determine the support reaction forces

We formulate the equilibrium equation:

$$\sum M_A = 0; \quad -G_2 \cdot 0.2 - q_1 \cdot 0.2 \cdot 0.1 + q_1 \cdot 1.6 \cdot 0.8 + q_2 \cdot 1.2 \cdot 0.7 + q_3 \cdot 1.2 \cdot 0.7$$
$$-R_B \cdot 1.4 + G_1 \cdot 1.6 - M + G_2 \cdot 1.7 = 0$$

$$R_B = \frac{-G_2 \cdot 0.2 - q_1 \cdot 0.2 \cdot 0.1 + q_1 \cdot 1.6 \cdot 0.8 + q_2 \cdot 1.2 \cdot 0.7}{1.4} + \frac{q_3 \cdot 1.2 \cdot 0.7 + G_1 \cdot 1.6 - M + G_2 \cdot 1.7}{1.4} = 0.859 \text{ kN}$$

$$\sum M_B = 0; \quad -G_2 \cdot 1.8 + q_1 \cdot 0.2 \cdot 0.1 - q_1 \cdot 1.6 \cdot 0.8 - q_2 \cdot 1.2 \cdot 0.7 - q_3 \cdot 1.2 \cdot 0.7 + R_A \cdot 1.4 + G_1 \cdot 0.2 - M + G_2 \cdot 0.3 = 0$$

$$R_A = \frac{-G_2 \cdot 1.8 + q_1 \cdot 0.2 \cdot 0.1 - q_1 \cdot 1.6 \cdot 0.8 - q_2 \cdot 1.2 \cdot 0.7}{1.4} - \frac{q_3 \cdot 1.2 \cdot 0.7 + G_1 \cdot 0.2 - M + G_2 \cdot 0.3}{1.4} = 1.177 \text{ kN}$$

Check: $\sum Y = 0$; $R_A + R_B - q_1 \cdot 1.8 - q_2 \cdot 1.2 - q_3 \cdot 1.2 - G_1 - 2G_2 = 0$;

$1.177 + 0.859 - 0.586 \cdot 1.8 - 0.416 \cdot 1.2 - 0.216 \cdot 1.2 - 0.14 - 2 \cdot 0.0174 = 0$;

$2.036 - 2.0374 = 0$

2) Determine the stiffness

To determine the stiffness, we use the universal equations for:

a) for the angle of rotation

$$\theta = \theta_0 + \frac{1}{EJ_y}\left[\sum M(x-a) + \frac{\sum P(x-b)^2}{2} + \frac{\sum q(x-c)^3}{6} - \frac{\sum q(x-d)^3}{6}\right]$$

b) to determine coolness

$$Z = Z_0 + \theta_0 x + \frac{1}{EJ_y}\left[\frac{\sum M(x-a)^2}{2} + \frac{\sum P(x-b)^3}{6} + \frac{\sum q(x-c)^4}{24} - \frac{\sum q(x-d)^4}{24}\right]$$

Boundary conditions:

$x = 0$	$x = 2.37$
$\theta_0 \neq 0$	$\theta_B \neq 0$
$z_0 = 0$	$z_B = 0$

Based on the obtained values, deformation (Q, M_u, and Z) plots were constructed using the "MathCad" program.

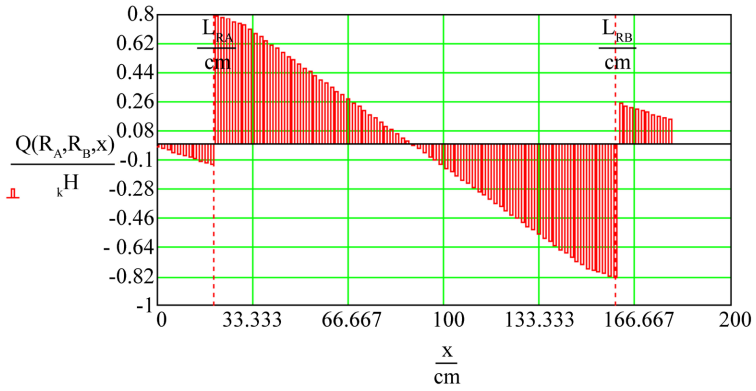

Figure 9. Cutting force graph on a resource-saving shaft.

The graph in Figure 9 shows the change in the shear force Q(x) along the resource-saving shaft. It can be seen from the graph that the points RA and RB, where the rods are located, have jumps in the values of the shear force, which represent the support reactions. In the range $0 \le x \le 100$ cm, the shear force has positive values and has a linear decreasing behavior, and at the point $x \approx 100$ cm, $Q(x) = 0$, which corresponds to the extremum of the bending moment at this point. In the range $100 \le x \le 166.7$ cm, the shear force takes on negative values and increases gradually.

Thus, the point where the shear force is equal to zero indicates that the shaft is the section where the greatest bending moment occurs.

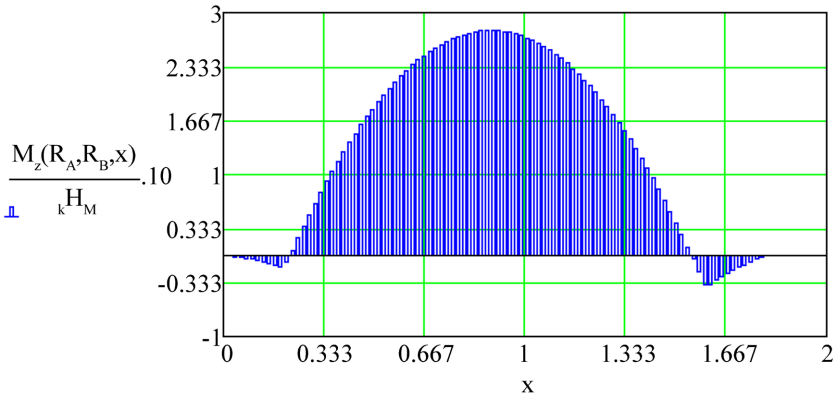

Figure 10. Graph of bending moment on the shaft.

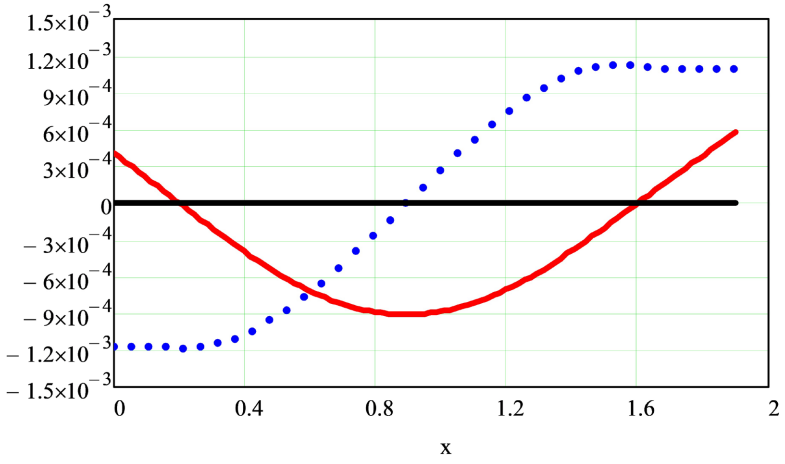

Figure 11. Diagrams of normal and equivalent stresses.

The graph in Figure 10 shows the distribution of the bending moment Mz (x) along the resource-saving shaft. The graph has a parabolic shape, which indicates a uniform distribution of the load acting on the resource-saving shaft. The maximum positive value of the bending moment is observed at approximately $x \approx 1$ m, which corresponds to the point where Q (x) = 0 on the shear force diagram. The value of the bending moments of the supports is equal to or close to zero, which

corresponds to the boundary condition.

The graphs constructed in the MathCad environment (Figure 11) confirm the consistency and stability of the results obtained based on theoretical calculations and demonstrate the suitability of the developed mathematical model for practical application.

3. Conclusions

Analysis of bending moments and displacement diagrams from the analysis of the bending strength of the saw drum shaft under load clearly reflects the deformation process of the shaft.

The constructed diagrams show that in rigidly supported shafts, the maximum bending moments are concentrated mainly in the support areas, while in freely supported shafts, the largest moment values are formed in the central part. This confirms that the type of support directly affects the location of stresses.

According to the displacement diagrams, the greatest deflection of the shaft is observed in zones with intensive load effects. In the rigidly supported case, the amount of displacement decreases, and the overall stiffness of the structure increases. In the freely supported case, the deformation is relatively large, which indicates increased requirements for strength in the operating mode.

The diagrams of normal and equivalent stresses made it possible to identify the most dangerous sections of the shaft. According to the results of the diagrams, it was found that the maximum tensile stresses occur in different zones in different fastening conditions. This is important in material selection and safety margin determination. The graphs constructed in the MathCad environment confirm the consistency and stability of the results obtained based on theoretical calculations and demonstrate the suitability of the developed mathematical model for practical application.

Conflicts of Interest

The authors declare no conflicts of interest regarding the publication of this paper.

References

[1] Abdurasulov, A., Akramova, D., Obidov, A., Mamazhanov, Sh. and Mirzaumidov, A. (2023) Study of the Durability of the Drum for Separating Fibers from Cotton Waste. Intellectual Property Agency under the Ministry of Justice of the Republic of Uzbekistan (20231584) No. DGU 22958.

[2] Van Huan, N. (2017) Increasing the Bending Rigidity of Long Shafts by Surface Plastic Deformation. Ph.D. Thesis, Irkutsk State Technical University, 165 p.

[3] Abdurasulov, A., Obidov, A., Mirzaumidov, A. and Otaqo'ziyev, D. (2024) Deformation of the Shaft in Torsion and the Effect of Torsion along with Bending. *Scientific and Technical Journal Namangan Institute of Engineering and Technology*, **9**, 208-216.

[4] Abdurasulov, A., Muhammadsodiqova, O. and Mirzaumidov, A. (2024) Creating a Simplified Structure of the Linter Saw Cylinder Shaft. *Namangan Engineering and Construction Institute Scientific Journal of Mechanics and Technology*, No. 4, 42-48.

[5] Rashidov, T.R., Shoziyotov, Sh. and Muminov, K. (1990) Fundamentals of Theoretical Mechanics. Ukituvchi, 497-504.

[6] Abdurasulov, A., Obidov, A., Mirzaumidov, A. and Yunisov, S. (2024) Research of the Shaft of the New Modernized Saw Cylinder Wall. No. 2, Ministry of Higher Education, Science and Innovations of the Republic of Uzbekistan, 249-255.

[7] Abdurasulov, A., Obidov, A. and Mirzaumidov, A. (2025) A Study of Critical Speed of Linter Shaft Rotation and Resonance Phenomenon. *Scientific and Technical Journal Namangan Institute of Engineering and Technology*, **10**, 202-210.

[8] Abduvakhidov, M.M. (2021) Study of the Issues of Determining the Parameters of Bending Rigidity of Saw Working Elements. Ph.D. Thesis, Namangan Engineering Technological Institute, 123 p.

[9] Yunusov, S.Z. (2017) Development of Efficient Designs and Improvement of the Scientific Foundations for Calculating the Parameters of Working Elements and Mechanisms of Saw Gins. Ph.D. Thesis, Tashkent Institute of Textile and Light Industry, 243 p.

[10] Mirzaumidov, A. (2019) Development of a Lightweight Design of a Gin Saw Cylinder. *NamMTI Ilmiy Tekhnika Zhurnal*, No. 4, 123-128.